Noncollinear magnetic structure and magnetoelectric coupling in buckled honeycomb $Co_4Nb_2O_9$: A single-crystal neutron diffraction study

Lei Ding,[1] Minseong Lee,[2,3] Tao Hong,[1] Zhiling Dun,[4] Ryan Sinclair,[4] Songxue Chi,[1] Harish K. Agrawal,[1] Eun Sang Choi,[2] Bryan C. Chakoumakos,[1] Haidong Zhou,[4,2] and Huibo Cao[1,*]

[1]*Neutron Scattering Division, Oak Ridge National Laboratory, Oak Ridge, Tennessee 37831, USA*
[2]*National High Magnetic Field Laboratory, Florida State University, Tallahassee, Florida 32306-4005, USA*
[3]*Department of Physics, Florida State University, Tallahassee, Florida 32306-3016, USA*
[4]*Department of Physics and Astronomy, University of Tennessee, Knoxville, Tennessee 37996-1200, USA*

(Received 24 February 2020; revised 4 September 2020; accepted 9 November 2020; published 30 November 2020)

Through an analysis of single-crystal neutron diffraction data, we present the magnetic structure and magnetoelectric properties of $Co_4Nb_2O_9$ under various magnetic fields. In zero field, neutron diffraction experiments below $T_N = 27$ K reveal that the Co^{2+} moments order in the (ab) plane without any spin canting along the c axis, manifested by the magnetic symmetry $C2/c'$. Along each Co chain parallel to the c axis, the moments of nearest-neighbor Co atoms order ferromagnetically with a small cant away from the next-nearest-neighbor Co moments. Under the applied magnetic field $H \parallel a$, three magnetic domains were aligned with their major magnetic moments perpendicular to the magnetic field with no other observable magnetic transitions. The influences of magnetic fields on the magnetic structures associated with the observed magnetoelectric coupling are discussed.

DOI: 10.1103/PhysRevB.102.174443

I. INTRODUCTION

The cross coupling of magnetization and electric polarization to their conjugate magnetic and electric field, well known as the magnetoelectric (ME) effect [1,2], has drawn a great deal of interest due not only to its essential role in the quest for emergent states of matter [3,4] and novel types of ferroic order [5–8] in condensed matter physics but also potential applications in spintronics [6,9–12]. The microscopic mechanisms underpinning the ME effect remain hitherto unsettled but basically they are restricted by symmetry [1,5]. Group theory requires that specific symmetry elements, namely spatial inversion and time reversal, have to be broken to make the ME effect active. Such symmetry restrictions are also applicable to a novel ferrotoroidic order that is related to the antisymmetric part of the linear ME tensor [7,8]. Materials showing ferrotoroidicity are elusive and a few typically proposed and investigated systems are the metal orthophosphates such as $LiCoPO_4$ [13], $MnPS_3$ [14], and the pyroxenes such as $CaMnGe_2O_6$ [15] and $LiFeSi_2O_6$ [16].

Recently, a corundum-type compound, $Co_4Nb_2O_9$, has been found to show both a large ME and magnetodielectric effect below the Néel temperature $T_N \approx 27$ K [17–21]. More interestingly, both the electric-field-induced magnetization and magnetic field controlled polarization have been experimentally observed on a powder sample [18,19]. $Co_4Nb_2O_9$ crystallizes with an α-Al_2O_3-type trigonal crystal structure with the space group $P\bar{3}c1$ [22] [see Fig. 1(a)] and can be viewed as a derivative of Cr_2O_3, one of the first predicted and discovered, and intensively studied room-temperature ME materials [23–27]. The magnetic structure of $Co_4Nb_2O_9$ was first determined by Bertaut *et al.* [22,28] to have antiferromagnetically coupled ferromagnetic Co^{2+} chains with the moments along the c axis. The determined magnetic symmetry allows a linear ME effect but is incompatible with the magnetoelectric effect recently measured on a single crystal [20]. Recently, a different magnetic structure, in which all spins are nearly parallel to the $[1\bar{1}0]$ direction with a canting along the c axis, was suggested based on a single-crystal neutron diffraction experiment [20]. Later on, Deng *et al.* argued another distinct magnetic structure without any spin canting to the c axis from powder neutron diffraction data [29].

Moreover, different spin-flop behaviors have been observed in $Co_4Nb_2O_9$ at a relatively small magnetic field of 0.2 T along the $[1\bar{1}0]$ direction in a single-crystal sample [20] and 1.2 T in a powder sample [18,19]. Then, conjectured magnetic structures associated with these magnetic anomalies have been suggested to explain the large ME and magnetodielectric effect [18,20]. More interestingly, Khanh *et al.* have found that the electric polarization vector can be promptly controlled by applying an in-plane magnetic field [30]. They attributed this effect to the continuous rotation of the antiferromagnetic moments on the honeycomb lattice.

To understand the large ME effect, one has to know the precise magnetic structure especially in such complex systems where magnetic properties are dominated by both the exchange interactions and single-ion anisotropy [29]. The magnetic structures in magnetic fields, which may explain the robust manipulation of the electric polarization by a magnetic field, remain unknown. In light of this, we set out to revisit the magnetic and magnetoelectric effect of $Co_4Nb_2O_9$ in different

*caoh@ornl.gov

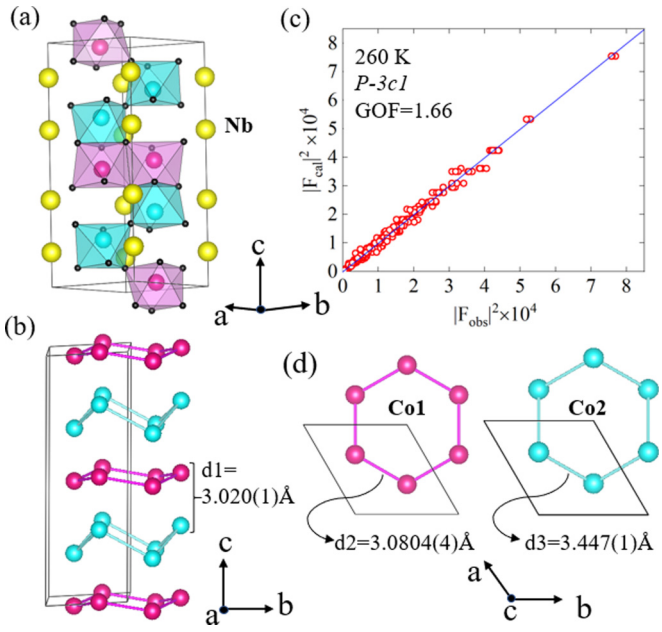

FIG. 1. (a) The crystal structure of $Co_4Nb_2O_9$ at room temperature. Co1 and Co2 atoms (pink and cyan spheres, respectively) are shown within their octahedral oxygen (black spheres) coordination. Nb atoms are represented by yellow large spheres. (b) and (d) highlight the buckled Co1 and Co2 honeycomb layers that are stacked along the *c* axis with the marked essential bonding distances between Co atoms. (c) Results of the crystal structure refinement from x-ray diffraction data at 260 K.

magnetic fields on a well-characterized high-quality single crystal.

In this paper, we report the detailed magnetic and magnetoelectric properties measured on a high-quality $Co_4Nb_2O_9$ single crystal and the evolution of magnetic structures with temperature and magnetic field measured by single-crystal neutron diffraction. We show that at zero magnetic field, single-crystal neutron diffraction data unveil a magnetic structure with the ordered moments confined in the *ab* plane, which allows a linear ME effect as further confirmed by the electric polarization measurements. We discuss the influence of magnetic field on the ME effect with neutron diffraction data under various magnetic fields.

II. EXPERIMENTAL METHODS

Single crystals of $Co_4Nb_2O_9$ were grown by the traveling-solvent floating-zone (TSFZ) technique. The feed and seed rods for the crystal growth were prepared by a solid state reaction. Appropriate mixtures of $CoCO_3$ and Nb_2O_5 were ground together and pressed into 6 mm diam × 60 mm rods under 400 atm hydrostatic pressure and then calcined in air at 1000 atm for 24 h. The crystal growth was carried out in argon in an IR-heated image furnace (NEC) equipped with two halogen lamps and double ellipsoidal mirrors with feed and seed rods rotating in opposite directions at 25 rpm during crystal growth at a rate of 4 mm/h.

Single-crystal x-ray diffraction data were collected at 260 K using a Rigaku XtaLAB PRO diffractometer with graphite monochromated Mo $K\alpha$ radiation ($\lambda = 0.710\,73$ Å) equipped with a Dectris Pilatus 200 K detector and an Oxford N-HeliX cryocooler. Peak indexing and integration were done using the RIGAKU OXFORD DIFFRACTION CRYSALISPRO software [31]. An empirical absorption correction was applied using the SCALE3 ABSPACK algorithm as implemented in CRYSALISPRO [32]. Structure refinement was done using FULLPROF suite [33].

The dc magnetization curves were obtained using a high-field vibrating sample magnetometer (VSM) of the National High Magnetic Field Laboratory. For the ac susceptibility measurement, the conventional mutual inductance technique was used with frequencies below 1000 Hz. Two balanced sensing coils were prepared and the sample was inserted into one of the two sensing coils. When the sample was magnetized by a small ac magnetic field superimposed on an external dc magnetic field, the magnetic susceptibility signal appears as unbalanced voltages across the sensing coils, which were measured using lock-in amplifiers.

For the dielectric constant and the electric polarization measurements, single-crystal samples were used and the orientations were determined by Laue diffraction. Two single-crystalline samples were polished to achieve two parallel flat surfaces perpendicular to the *a* axis and the *c* axis. The dimensions were $1.8 \times 1.8 \times 0.3$ and $2.2 \times 2.2 \times 0.4$ mm^3, respectively. An Andeen-Hagerling AH-2700A commercial capacitance bridge was used to measure the capacitance, which was converted to the dielectric constant using the relation between the capacitance and an infinite parallel capacitor. The electric polarization was obtained by integrating the pyroelectric current (I_p) with respect to time. The I_p was measured during warmup after the sample was cooled in the presence of a poling electric field and/or external magnetic field. The detailed procedure can be found in Ref. [34].

Single-crystal neutron diffraction was performed at the HB-3A four-circle diffractometer (FCD) equipped with a two-dimensional (2D) detector at the High Flux Isotope Reactor (HFIR) at Oak Ridge National Laboratory (ORNL). A neutron wavelength of 1.003 Å (neutron energy 81 meV) was used with a bent perfect Si-331 monochromator [35]. The nuclear and magnetic structure refinements were performed with the FULLPROF suite [33]. Single-crystal neutron diffraction under various magnetic fields was measured at a cold neutron triple axis spectrometer (CTAX) at HFIR at ORNL. A neutron wavelength of 4.045 Å (neutron energy 5 meV) was used.

III. RESULTS

A. Crystal structure

In view of the inconclusive magnetic structure and the debatable spin-flop behavior of $Co_4Nb_2O_9$, it is important to examine the as-grown crystals as effects such as crystal domains, impurities, or defects can often give rise to unpredictable and spurious results. Hence we first carefully characterized our single crystals using x-ray single-crystal diffraction. The crystal structure was solved and refined based on the x-ray single-crystal diffraction data at 260 K as described in the experimental section. More than 2290 reflections (effective reflections 560 with $I > 4\sigma$) were used

TABLE I. The structure parameters of $Co_4Nb_2O_9$ measured at 260 K by single-crystal x-ray diffraction. The space group is $P\bar{3}c1$, $a = 5.1877(4)$ Å, $b = 5.1877(4)$ Å, $c = 14.1841(4)$ Å, $\alpha = 90°$, $\beta = 90°$, $\gamma = 120°$. $R_f = 3.2\%$. $\chi^2 = 1.66$. The anisotropic atomic displacement parameters U_{ij} in Å^2.

Atom	Type	Site	x	y	z	U_{11}	U_{22}	U_{33}	U_{12}	U_{13}	U_{23}
Nb1	Nb	4c	0	0	0.3578(1)	0.0079(8)	0.0079(8)	0.004(1)	$U_{11}/2$	0	0
Co1	Co	4d	1/3	2/3	0.0138(3)	0.007(2)	0.007(2)	0.0012(3)	$U_{11}/2$	0	0
Co2	Co	4d	1/3	2/3	0.3071(2)	0.007(2)	0.007(2)	0.013(2)	$U_{11}/2$	0	0
O1	O	6f	0.297(3)	0	1/4	0.015(8)	0.004(8)	0.007(6)	$U_{22}/2$	−0.001(5)	−0.001(5)
O2	O	12g	0.342(1)	0.309(3)	0.0838(7)	0.011(6)	−0.012(4)	0.014(4)	0.005(4)	0.007(5)	0.005(4)

in the structure refinements. It shows that $Co_4Nb_2O_9$ crystallizes with the space group $P\bar{3}c1$, in good agreement with the previous report [22]. The single crystal was practically perfect without suffering from twins, impurities, and significant defects. The data fit quality is shown in Fig. 1(c) with a comparison between the observed squared structure factor and the calculated one with a goodness-of-fit value of 1.66.

We further measured the $Co_4Nb_2O_9$ single crystal using single-crystal neutron diffraction at 50 K which confirms the space group $P\bar{3}c1$ and reveals a good quality of the single crystal. The structural parameters from the refinement of single-crystal x-ray and neutron diffraction data are summarized in Tables I and II, respectively. As presented in Fig. 1, the crystal structure consists of an alternate stacking of slightly buckled Co1 honeycomb and buckled Co2 honeycomb layers along the c axis. Even though $Co_4Nb_2O_9$ features a stacking of honeycomb layers, the nearest-neighbor bonding between Co cations is the Co1-Co2 bond [$d1 = 3.020(1)$Å] along the c axis as marked in Fig. 1(b). The nearest bonding between Co atoms within each honeycomb layer is $d2 = 3.0804(4)$ Å and $d3 = 3.447(1)$ Å for Co1-Co1 and Co2-Co2 bonds, respectively [Fig. 1(d)].

B. Magnetic and magnetoelectric properties

A magnetic susceptibility measurement shows that $Co_4Nb_2O_9$ undergoes an antiferromagnetic transition at $T_N = 27$ K, characterized by a sharp cusp in the susceptibility curve (Fig. 2), in accordance with previous results [20]. The Curie-Weiss fit of the inverse susceptibility data from 175 to 300 K yields an effective moment $5.0\mu_B$ that indicates the high spin state for Co^{2+} with $S = 3/2$. To characterize the magnetic phase transition, we have for the first time measured the heat capacity of $Co_4Nb_2O_9$. It reveals a sharp peak in the heat capacity curve, reflecting the nature of long-range spin order [Fig. 2(a)].

TABLE II. The structure parameters of $Co_4Nb_2O_9$ measured at 50 K by single-crystal neutron diffraction. The space group is $P\bar{3}c1$, $a = 5.180(3)$ Å, $b = 5.180(3)$ Å, $c = 14.163(6)$ Å, $\alpha = 90°$, $\beta = 90°$, $\gamma = 120°$. $R_f = 4.51\%$. $\chi^2 = 3.64$. The atomic displacement parameter U_{iso} in Å^2.

Atom	Type	Site	x	y	z	U_{iso}
Nb1	Nb	4c	0	0	0.3572(6)	0.005
Co1	Co	4d	1/3	2/3	0.018(1)	0.005
Co2	Co	4d	1/3	2/3	0.3068(9)	0.005
O1	O	6f	0.296(3)	0	1/4	0.008
O2	O	12g	0.346(2)	0.303(3)	0.0842(8)	0.008

Isothermal magnetization measurements at high magnetic fields were carried out at 1.5 K up to 35 T along both the a axis and the c axis. No magnetic saturation was observed. The magnetization along the a axis is evidently higher than that along the c axis, suggesting an easy-plane magnetic anisotropy [20]. Up to 10 T, the magnetization along both the a and c axes show a near linear behavior. The ac magnetic sus-

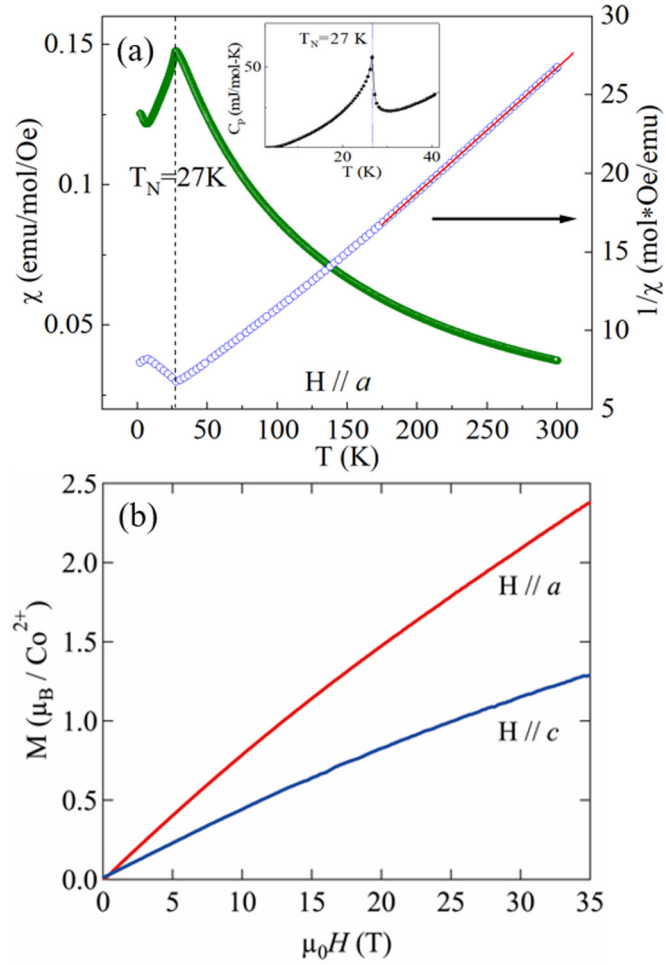

FIG. 2. (a) The magnetic susceptibility of $Co_4Nb_2O_9$ as a function of temperature with $\mu_0 H = 0.1$ T parallel to the a axis. The inset shows the temperature-dependent heat capacity of $Co_4Nb_2O_9$. (b) The isothermal magnetization curves at 1.5 K with magnetic field up to 35 T.

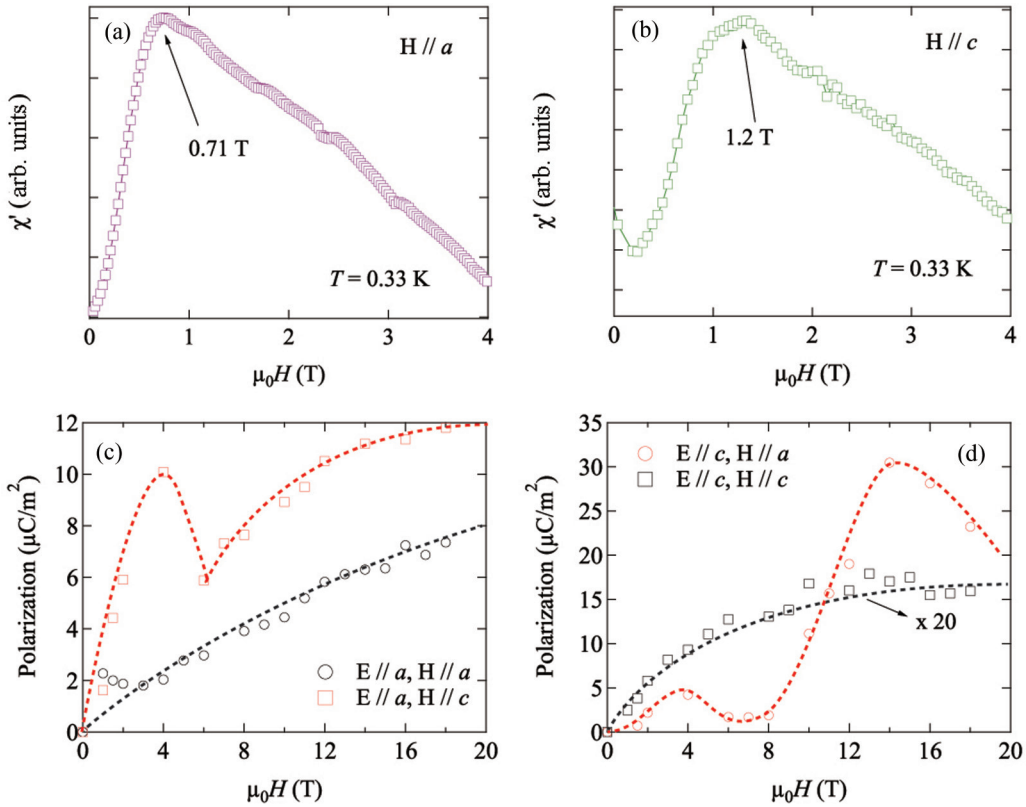

FIG. 3. (a) and (b) The magnetic-field-dependent ac susceptibility with H parallel to the a and c axes at 0.33 K, respectively. (c) and (d) The magnetic field dependence of electric polarization at 21.5 K with different magnetoelectric annealing configurations. The lines in (c) and (d) are guides to the eye.

ceptibilities as a function of magnetic field were measured at various temperatures with the applied magnetic field parallel to the a and c axes. As shown in Figs. 3(a) and 3(b), the ac susceptibility curves at $T = 0.33$ K reveal two critical magnetic fields of 0.71 and 1.2 T along the a and c axes, respectively. Such anomalies were tentatively explained as "spin-flop" behavior in the earlier reports [18,19,36]. However, as we concluded by our field-dependent neutron diffraction data later, these features are attributed to a combined consequence of the alignment of magnetic domains and spin rotations.

To detect the magnetoelectric effect, the electric polarization of $Co_4Nb_2O_9$ single crystal was measured under various magnetic and electric fields along the a or c axes after completing the magnetoelectric annealing procedure [15]. Detailed field-induced pyroelectric current and electric polarization curves as a function of temperature at various magnetic fields are shown in Figs. 7 and 8 in the Appendix. Figures 3(c) and 3(d) show the magnetic-field-dependent electric polarization measured at 21.5 K using electric fields $E = 320$ and 260 kV/m, respectively. When the applied magnetic field is perpendicular to the electric field, the value of polarization increases linearly below 4 T with an increase of magnetic field. However, a steep drop sets in around the applied magnetic field of 4 T. This is likely associated with the procedure of the alignment of magnetic domains as explained in the following. Above this magnetic field, electric polarization restores the linear behavior. It is clear that when both the magnetic and electric field are applied in the same direction, either the a or c axis, a relatively smaller polarization is observed. This indicates that the off-diagonal ME tensor components have larger values than the diagonal ones, allowed by the magnetic symmetry $C2/c'$ (see the neutron diffraction section). Evidently, the magnetoelectric properties in $Co_4Nb_2O_9$ are distinct from that in Cr_2O_3 where only the diagonal ME tensor terms were observed below the spin-flop field imposed by its magnetic symmetry $P\bar{3}'m'$ [24,37]. Therefore, such an observation reflects that the previously documented magnetic structure with the magnetic point group $-3'm'$ which allows only diagonal terms is inappropriate [22,28].

C. Zero-magnetic-field single-crystal neutron diffraction

We performed single-crystal neutron diffraction to revisit the magnetic structure of $Co_4Nb_2O_9$ down to 5 K. As shown in Fig. 4, several selected Bragg reflections were measured to track the magnetic phase transition upon warming. One can clearly see the increased intensity for the representative reflections (004), (200), (113), (104), and (001) below T_N. This indicates that all the magnetic reflections can be well indexed by a propagation vector $\mathbf{k} = \mathbf{0}$, as reported in Refs. [20,29]. No further crystal structure transition was detected down to 5 K.

A symmetry analysis was performed to determine the magnetic structures of $Co_4Nb_2O_9$. A number of magnetic subgroups that are compatible with the given space group and propagation vector can be calculated by Bilbao

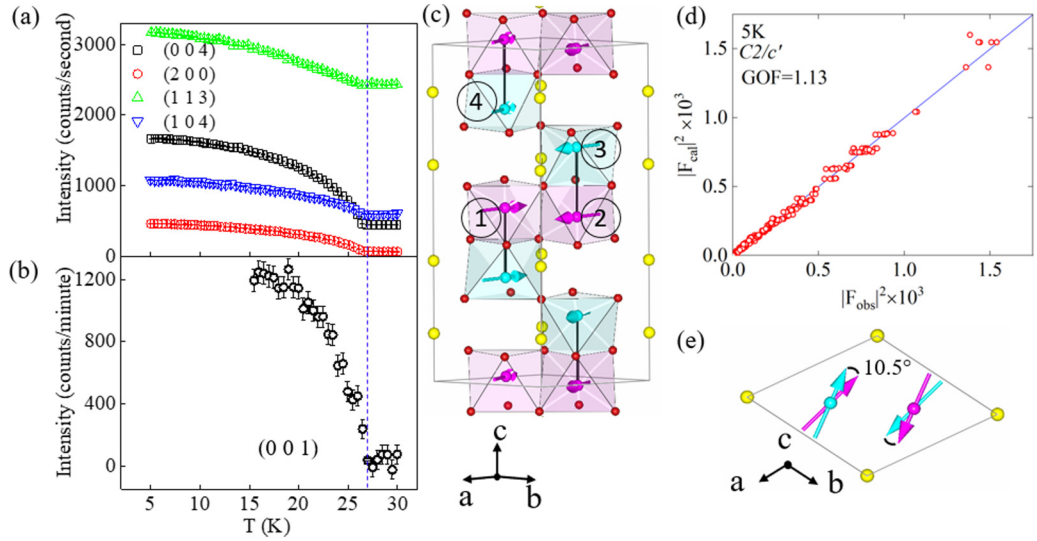

FIG. 4. (a) and (b) The representative magnetic reflections as a function of temperature reflecting the magnetic phase transition at 27 K. The data were measured at HB-3A with a neutron wavelength of 1.003 Å. (c) The magnetic structure of $Co_4Nb_2O_9$ showing the ferromagnetically coupled Co1-Co2 pairs connected by the solid lines (the nearest-neighbor Co1 and Co2 atoms in each chain). Labels 1–4 in a circle denote the representative spins (for details, see the discussion section). (d) Results of the magnetic structure refinement for the neutron data collected at 5 K. (e) All spins are confined in the *ab* plane with the canting angle between Co1 and Co2 spins (the next-nearest neighbor along the *c* axis).

Crystallographic Server (magnetic symmetry and applications [38]) software. The magnetic structures bearing trigonal symmetry imply the magnetic moments along the c axis, inconsistent with our experimentally measured magnetic reflections such as (004) and (001). Therefore, we have to lower the symmetry from the k-maximal magnetic symmetry in the subgroup hierarchy. We then found the monoclinic magnetic subgroups $C2'/c'$, $C2/c'$, $C2'/c$, and $C2/c$. The observed magnetic reflections also imply that spins should be confined into the *ab* plane, distinct from a previous report where a magnetic moment component out of the *ab* plane was found [20]. Since the magnetic peaks superpose on the nuclear reflections below T_N, a combined magnetic and nuclear structure refinement was performed. The refinement using $C2/c'$ magnetic space group yields the best fitting with $R_f = 6.4\%$ and $\chi^2 = 1.13$ for the combined phase for 745 reflections. The results of the refinement and the corresponding illustrations of magnetic structure are shown in Fig. 4. The magnetic structure solved can be simply viewed as antiferromagnetically coupled ferromagnetic chains along the c axis. Magnetic moments in each chain are confined into the *ab* plane with ferromagnetic pairs for the nearest-neighbor Co1 and Co2 atoms and a canting angle 10.5° between the next-nearest-neighboring Co1-Co2 spins in the chain. The refined ordered magnetic moment is $2.820(8)\mu_B$ [$m_x = 3.201(8)\mu_B$, $m_y = 2.12(1)\mu_B$] for both the Co1 and Co2 sites. Given the magnetic symmetry allows the magnetic component along the c axis, we have also examined this possibility. The refinement indicates that the value of m_z is minimal and beyond the resolution limit of the present neutron diffraction experiment. The magnitude of the ordered magnetic moment for Co^{2+} is close to the theoretical spin-only ordered value $3\mu_B$ for Co^{2+} with a high spin state, indicating that the orbital moment is nearly quenched as shown in Refs. [39,40]. Note that due to the existence of the trigonal lattice symmetry, three magnetic domains were considered and their populations were set to be equal during the refinement. In the following, we show that the population of magnetic domains in $Co_4Nb_2O_9$ can be tuned by applying an external magnetic field.

The magnetic symmetry can also be readily derived by the observed magnetoelectric coupling. By applying the Neumann's principle to the magnetoelectric effect with these possible magnetic symmetries, we could exclude the subgroups $C2'/c'$ and $C2/c$. This is because, in principle, neither of them allows the presence of the linear ME effect. The $C2'/c'$ and $C2/c$ subgroups do not necessarily mean a ferromagnetic structure (in other words, there is no symmetry constraint for a ferromagnetic arrangement); hence this is not the reasoning that we ruled them out [20]. The observed ME properties can help us preclude the $C2'/c$ subgroup since this symmetry allows only the off-diagonal terms. Thereby, the only magnetic subgroup compatible with $Co_4Nb_2O_9$ is $C2/c'$ based on our symmetry analysis and experimental observations, in good agreement with the neutron diffraction results.

D. Single-crystal neutron diffraction in magnetic fields

To clarify the hidden mechanism of the complex ME effect in $Co_4Nb_2O_9$, we carried out neutron diffraction experiments under high magnetic fields at CTAX. The same crystal used at HB-3A was measured in the $(0KL)$ scattering plane. The crystal misalignment was less than 1° for this experiment. The magnetic field was applied vertically, i.e., along the crystal's a axis. The representative reflections were measured with rocking curve scans at selected temperatures under magnetic fields up to 10 T. The integrated magnetic intensities of these reflections are plotted versus the magnetic field in Figs. 5(a)–5(e). They were obtained by subtracting the integrated intensities at 50 K from that at 1.5 K. A considerable decrease in the

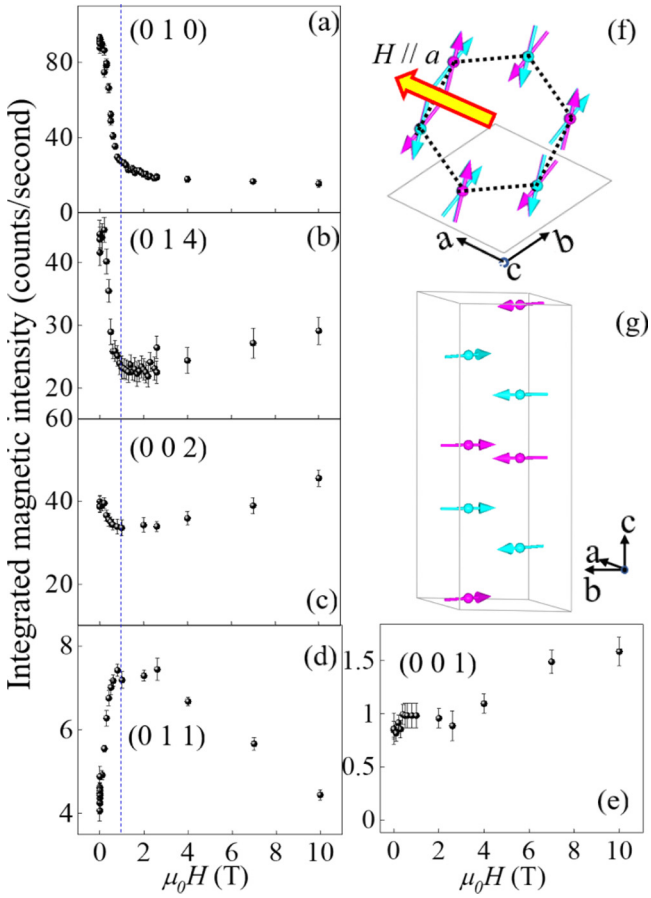

FIG. 5. (a)–(e) The selected magnetic reflections as a function of magnetic field along the a axis measured at CTAX. The solid line marks the alignment of magnetic domains. (f) and (g) The magnetic structure of $Co_4Nb_2O_9$ after the three magnetic domains are aligned. All the Co spins are nearly parallel to the b^* direction.

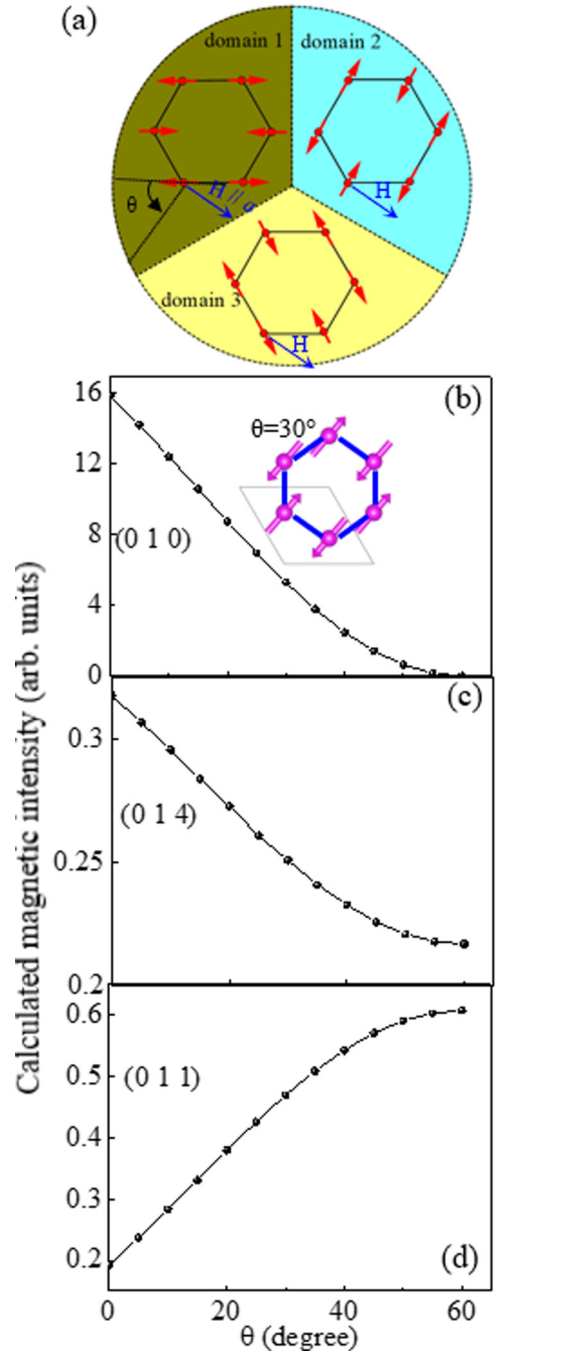

FIG. 6. (a) Schematic drawing of the spin configurations for the three symmetry-related magnetic domains. θ denotes the rotational angle of spins resulting from the magnetic field parallel to the a axis. (b)–(d) Calculated intensities for the magnetic reflections (010), (014), and (011) as a function of θ. The inset shows the spin configuration with the rotation angle of 30° in domain 1.

magnetic intensities of reflections (010) and (014) with the increasing magnetic field up to 1 T is observed whereas there is a significant increase in the intensity of magnetic reflection (011). There is only a slight decrease in the intensity of the magnetic peak (002). These changes indicate a spin reorientation from the trigonal lattice direction [100], [010], or [110] to the direction parallel to the reciprocal [010] direction (the b^* axis), which causes a large decrease of the magnetic scattering at (010) and (014) reflections but an evident increment of the (011) magnetic reflection. The magnetic intensities at 1 T were obtained by scaling them to those measured at zero magnetic field that was well solved with the complete data measured at HB-3A for catching all the necessary corrections. With the five magnetic reflections at 1 T, the magnetic structure with a single magnetic domain can fit the data in a satisfactory quality ($\chi^2 = 6.09$) and yields the moments along the [120] direction in real space and the [010] direction in reciprocal space (Fig. 5), in the same magnetic symmetry $C2/c'$ as that at zero magnetic field. The ordered magnetic moments are $2.6(1)\mu_B$ for both Co sites with a slightly increased planar canting angle of 12.2°. The above refinement did not consider the induced ferromagnetic moments along the a axis (the induced moments are small as expected from the magnetization measurements in Fig. 2).

The magnetic field 1 T $< \mu_0 H <$ 4 T does not greatly change the intensities of the magnetic reflections (010), (014), (002), (011), and (001), suggesting a rather robust magnetic ground state. Above 4 T, only the magnetic reflection (011) was appropriately suppressed while the intensities of

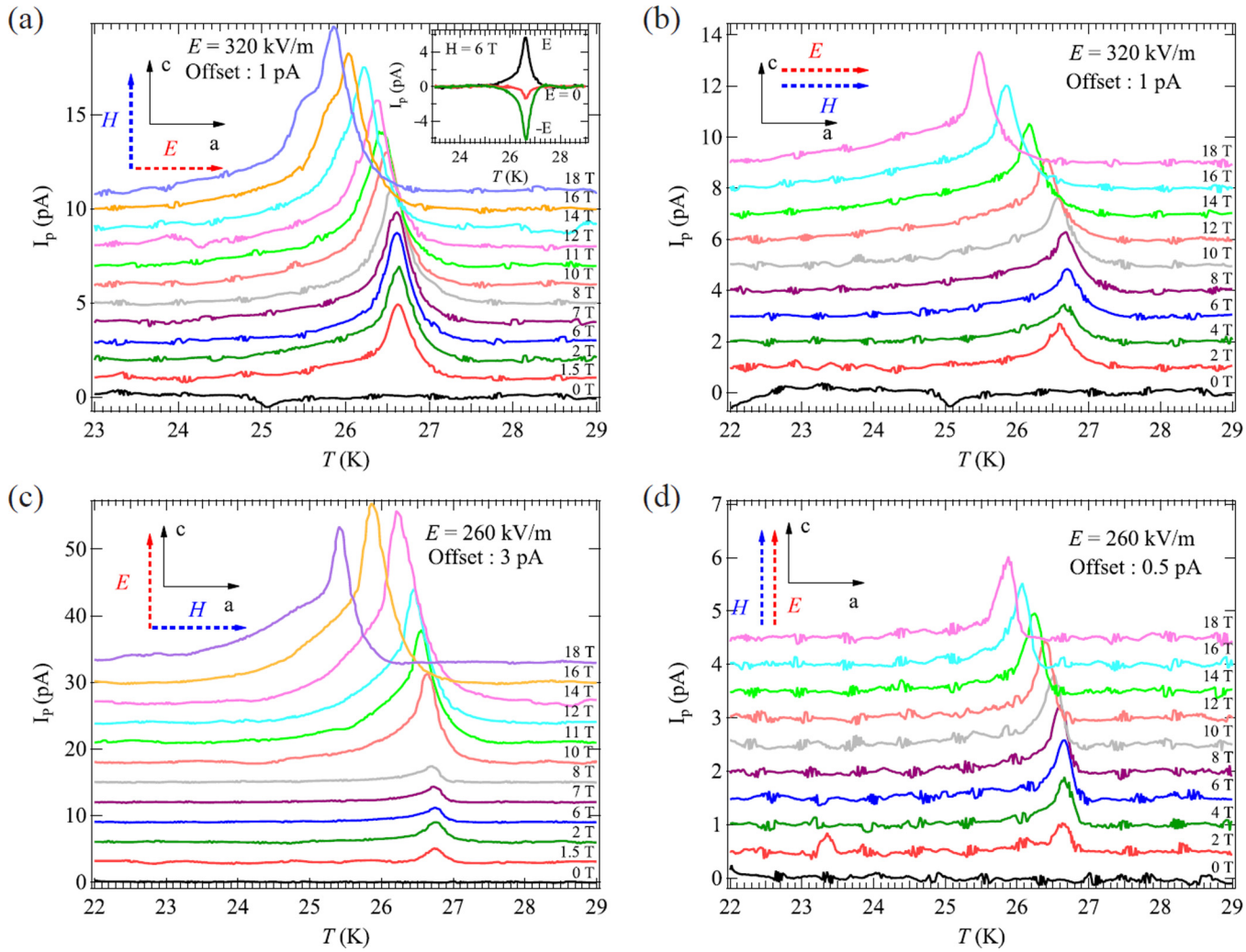

FIG. 7. Pyroelectric current (I_p) measured under poling field E and magnetic field H. Directions of the applied E and H are shown by arrows along either the a or c axis.

the reflections (014) and (002) slightly increase. This may be due to a small induced ferromagnetic component under high magnetic fields. This, along with the slight increase of the magnetic reflection (001) from 4 to 10 T, suggests no further occurrence of a magnetic phase transition but spin rotation in the *ab* plane. Indeed, by refining the observed magnetic reflections at 10 T using the magnetic symmetry obtained at 1 T, we arrived at a smaller planar canting angle 8.5° and magnetic moment $2.9(3)\mu_B$ for both sites. In the magnetic-field-dependent polarization curves, it is clear that a steep drop occurs around 4 T, correlating with the abrupt decrease of the observed magnetic reflection (011). In the magnetic field range of 6–14 T, it appears that the linear magnetoelectric effect is restored. The reason for the reentrant linear behavior is not obvious as there is no associated response in the intensities of the magnetic reflections. However, given the change of the value of the electric polarization is not significant, it seemingly supports our conclusion that a magnetic field up to 10 T does not break the magnetic symmetry but rotates the magnetic moments in the *ab* plane. The underlying mechanisms of the anomalies in the electric polarization at high magnetic fields deserve further study.

IV. DISCUSSION

We have shown that $Co_4Nb_2O_9$ antiferromagnetically orders below 27 K with the magnetic space group $C2/c'$ which allows a linear ME effect, consistent with previous reports by Khanh *et al.* [20] and Deng *et al.* [29]. However, in the former case, they found that all spins are exactly ferromagnetically aligned with a considerable canting angle 22° toward the c axis (mainly in the *ab* plane). This in fact is different from our results in which spin out of the *ab* plane is minimal based on our neutron diffraction data even though the m_z component is symmetry allowed. In the latter case, a distinct magnetic structure was reported where all moments are purely in the *ab* plane with in-plane canting angles of 1.3° and 25.2° for the neighbor Co1 and Co2 moments, respectively. By contrast, we deliver a magnetic structure akin to the latter case but with a different configuration by a careful neutron diffraction measurement on a high-quality single crystal. As illustrated in Fig. 4, the difference from the prior work is the presence of a ferromagnetic pair between the nearest-neighbor Co1 and Co2 atoms (labeled as atom 2 and atom 3 in Fig. 4) along the c axis and a planar canting angle between each adjacent Co1-Co2

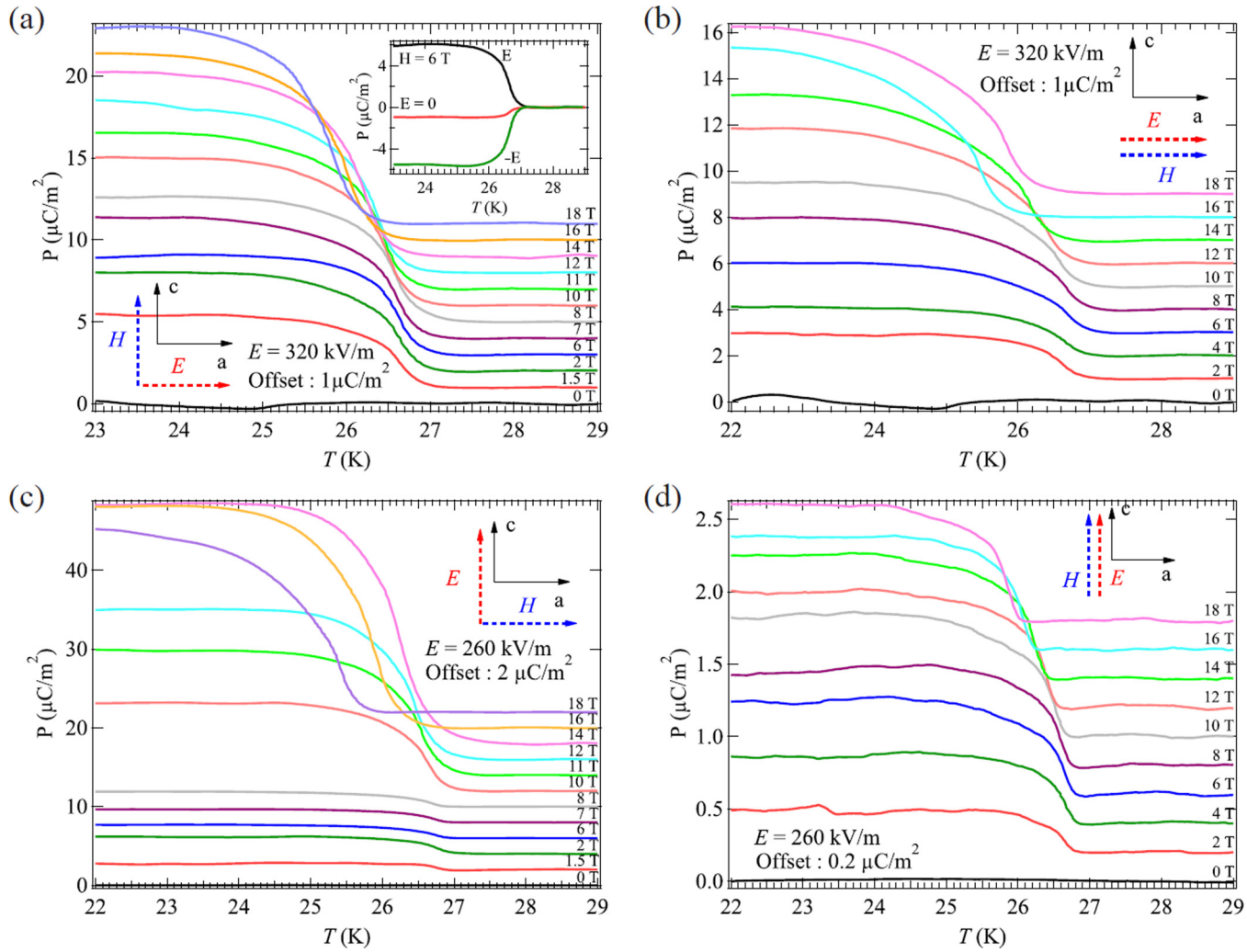

FIG. 8. Polarization data are obtained by integrating I_p shown in Fig. 7. Directions of the poling field E and magnetic field H are shown by arrows along either the a or c axis.

pair (the angle between atom 1 and atom 4 in Fig. 4). The presence of the canting angle in the ab plane is essentially supported by the observed (001) magnetic reflection. Our magnetic arrangement is likely more favored by the special crystal structural arrangement of Co atoms. The nearest-neighbor bond between Co atoms is Co1-Co2 along the c axis with a bond distance of $d1 = 3.020(1)$ Å as marked in Fig. 1(b) and a bond angle of Co1-O2-Co2 $= 83.3(2)^\circ$, giving rise to the strong exchange interaction mediating the edge-sharing $Co1O_6$ and $Co2O_6$ octahedra through superexchange interactions. Such an angle smaller than 90° principally indicates a strong ferromagnetic exchange interaction. The exactly antiparallel spin arrangement between the Co1 atoms in the slightly distorted honeycomb layer from our neutron diffraction experiment reflects a strong antiferromagnetic interaction. Actually, the conjectured exchange interactions are supported by a recent inelastic neutron scattering work [29] where they also suggested a rather large in-plane anisotropy and a considerable Dzyaloshinskii-Moriya interaction [41,42] in $Co_4Nb_2O_9$. The former coincides with the planar spin arrangement while the latter can naturally explain the canting angle between ferromagnetic pairs [29].

A magnetic field of 1 T along the a axis does not significantly change the moment size and the magnetic arrangement but simultaneously rotates and aligns the three magnetic domains to the single one with the spins perpendicular to the magnetic field. This elucidates the conjecture of "spin flop" in the previous works [18–20]. To make this point clear, we demonstrate the rotation of spins and the alignment process of the three magnetic domains. Figure 6(a) shows the relationship between the three magnetic domains in real space. θ denotes the rotational angle for the magnetic domain 1 correlating with the applied magnetic field. Starting from the magnetic structure in zero field, we can calculate the intensities of the magnetic reflections as a function of θ. As shown in Figs. 6(b)–6(d), the evolution of the significant magnetic reflections (010), (014), and (011) reproduces the change of them under magnetic field (Fig. 5). This consistency corroborates that the consequence of a magnetic field smaller than 4 T is a combination of the rotation of spins and the alignment of the three magnetic domains. In the magnetic field dependence of electric polarization curves, a sudden drop around 4 T is likely a result of the variation of the magnetic domains since thermally stimulated current sources in the course of magnetic

domain alignment may contribute to the pyroelectric current so as to modify the electric polarization [43,44]. Above 4 T, i.e., the system in a single magnetic domain, the observed magnetoelectric effect should be more intrinsic because the magnetic structure remains unaltered with the magnetic field up to 10 T. Such a robust magnetic symmetry in a magnetic field, that probably emanates from strong easy-plane single-ion anisotropy, provides a natural explanation for the manipulation of electric polarization [30,36].

The solved magnetic symmetry with its off-diagonal components non-null in $Co_4Nb_2O_9$ in principle allows for the occurrence of ferrotoroidal order. The experimental observation of the relevant ferrotoroidal domains through a magnetoelectric annealing process is greatly desired. This can be spatially resolved by optical second harmonic generation and a spherical neutron polarimetry determination of the relative domain populations [13,14].

V. CONCLUSION

We have investigated the magnetoelectric properties and magnetic structure evolution with temperature and magnetic field of a high-quality single crystal $Co_4Nb_2O_9$. Single-crystal neutron diffraction without a magnetic field revealed a magnetic structure below 27 K characterized by $C2/c'$ symmetry with magnetic moments totally confined in the *ab* plane, which allows the linear ME effect as observed experimentally by the pyroelectric current measurements. Single-crystal neutron diffraction in a magnetic field with $H \parallel a$ showed that the magnetization anomaly around 1 T is in fact a combination of the spin rotation and magnetic domain alignment driving the magnetic moments parallel to the b^* direction without breaking the magnetic symmetry. A higher magnetic field up to 10 T did not change the magnetic symmetry but rotates the magnetic moments in the *ab* plane. The robust magnetic structure under the external magnetic field offers a natural way to manipulate and control the electric polarization in this system.

ACKNOWLEDGMENTS

L.D. thanks J. Rodriguez-Carvajal for helpful discussions. The research at Oak Ridge National Laboratory (ORNL) was supported by the U.S. Department of Energy (DOE), Office of Science, Office of Basic Energy Sciences, Early Career Research Program Award No. KC0402010, under Contract No. DE-AC05-00OR22725. This research used resources at the High Flux Isotope Reactor, a DOE Office of Science User Facility operated by ORNL. The work at University of Tennessee was supported by DOE under Award No. DE-SC-0020254. A portion of this work was performed at the National High Magnetic Field Laboratory, supported by the National Science Foundation Cooperative Agreement No. DMR-1644779 and the State of Florida.

APPENDIX: POLARIZATION MEASUREMENTS OF $Co_4Nb_2O_9$

See Figs. 7 and 8 for electric polarization measurements.

[1] H. Schmid, Ferroelectrics **162**, 317 (1994).
[2] J.-P. Rivera, Eur. Phys. J. B **71**, 299 (2009).
[3] Y. Tokura, Science **312**, 1481 (2006).
[4] A. M. Essin, J. E. Moore, and D. Vanderbilt, Phys. Rev. Lett. **102**, 146805 (2009).
[5] M. Fiebig, J. Phys. D **38**, R123 (2005).
[6] Y. Tokura, S. Seki, and N. Nagaosa, Rep. Prog. Phys. **77**, 076501 (2014).
[7] N. A. Spaldin, M. Fiebig, and M. Mostovoy, J. Phys.: Condens. Matter **20**, 434203 (2008).
[8] H. Schmid, J. Phys.: Condens. Matter **20**, 434201 (2008).
[9] J. Wang, J. B. Neaton, H. Zheng, V. Nagarajan, S. B. Ogale, B. Liu, D. Viehland, V. Vaithyanathan, D. G. Schlom, U. V. Waghmare, N. A. Spaldin, K. M. Rabe, M. Wuttig, and R. Ramesh, Science **299**, 1719 (2003).
[10] N. A. Spaldin and M. Fiebig, The renaissance of magnetoelectric multiferroics, Science **309**, 391 (2005).
[11] W. Eerenstein, N. D. Mathur, and J. F. Scott, Nature (London) **442**, 759 (2006).
[12] S.-W. Cheong and M. Mostovoy, Nat. Mater. **6**, 13 (2007).
[13] B. B. Van Aken, J. P. Rivera, H. Schmid, and M. Fiebig, Nature (London) **449**, 702 (2007).
[14] E. Ressouche, M. Loire, V. Simonet, R. Ballou, A. Stunault, and A. Wildes, Phys. Rev. B **82**, 100408(R) (2010).
[15] L. Ding, C. V. Colin, C. Darie, J. Robert, F. Gay, and P. Bordet, Phys. Rev. B **93**, 064423 (2016).
[16] M. Baum, K. Schmalzl, P. Steffens, A. Hiess, L. P. Regnault, M. Meven, P. Becker, L. Bohatý, and M. Braden, Phys. Rev. B **88**, 024414 (2013).
[17] E. Fischer, G. Gorodetsky, and R. M. Hornreich, Solid State Commun. **10**, 1127 (1972).
[18] T. Kolodiazhnyi, H. Sakurai, and N. Vittayakorn, Appl. Phys. Lett. **99**, 132906 (2011).
[19] Y. Fang, Y. Q. Song, W. P. Zhou, R. Zhao, R. J. Tang, H. Yang, L. Y. Lv, S. G. Yang, D. H. Wang, and Y. W. Du, Sci. Rep. **4**, 3860 (2014).
[20] N. D. Khanh, N. Abe, H. Sagayama, A. Nakao, T. Hanashima, R. Kiyanagi, Y. Tokunaga, and T. Arima, Phys. Rev. B **93**, 075117 (2016).
[21] L. H. Yin, Y. M. Zou, J. Yang, J. M. Dai, W. H. Song, X. B. Zhu, and Y. P. Sun, Appl. Phys. Lett. **109**, 032905 (2016).
[22] E. F. Bertaut, L. Corliss, F. Forrat, R. Aleonard, and R. Pauthenet, J. Phys. Chem. Solids **21**, 234 (1961).
[23] I. E. Dzyaloshinskii, Zh. Exp. Teor. Fiz. **37**, 881 (1959); [Sov. Phys. JETP **10**, 628 (1960)].
[24] D. N. Astrov, Zh. Exp. Teor. Fiz. **38**, 984 (1960); [Sov. Phys. JETP **11**, 708 (1960)].
[25] A. Iyama and T. Kimura, Phys. Rev. B **87**, 180408(R) (2013).

[26] M. Fiebig, D. Frohlich, B. B. Krichevtsov, and R. V. Pisarev, Phys. Rev. Lett. **73**, 2127 (1994).
[27] T. R. McGuire, E. J. Scott, and F. H. Grannis, Phys. Rev. **102**, 1000 (1956).
[28] B. Schwarz, D. Kraft, R. Theissmann, and H. Ehrenberg, J. Magn. Magn. Mater. **322**, L1 (2010).
[29] G. Deng, Y. Cao, W. Ren, S. Cao, A. J. Studer, N. Gauthier, M. Kenzelmann, G. Davidson, K. C. Rule, J. S. Gardner, P. Imperia, C. Ulrich, and G. J. McIntyre, Phys. Rev. B **97**, 085154 (2018).
[30] N. D. Khanh, N. Abe, S. Kimura, Y. Tokunaga, and T. Arima, Phys. Rev. B **96**, 094434 (2017).
[31] Rigaku, Crystal Clear (2005), Rigaku Corporation, Tokyo, Japan.
[32] T. Higashi, ABSCOR (2000), Rigaku Corporation, Tokyo, Japan.
[33] J. Rodriguez-Carvajal, Physica B **192**, 55 (1993).
[34] M. Lee, J. Hwang, E. S. Choi, J. Ma, C. R. Dela Cruz, M. Zhu, X. Ke, Z. L. Dun, and H. D. Zhou, Phys. Rev. B **89**, 104420 (2014).
[35] B. C. Chakoumakos, H. Cao, F. Ye, A. D. Stoica, M. Popovici, M. Sundaram, W. Zhou, J. S. Hicks, G. W. Lynn, and R. A. Riedel, J. Appl. Crystallogr. **44**, 655 (2011).
[36] I. V. Solovyev and T. V. Kolodiazhnyi, Phys. Rev. B **94**, 094427 (2016).
[37] L. M. Corliss, J. M. Hastings, R. Nathans, and G. Shirane, J. Appl. Phys. **36**, 1099 (1965).
[38] J. M. Perez-Mato, S. V. Gallego, E. S. Tasci, L. Elcoro, G. de la Flor, and M. I. Aroyo, Annu. Rev. Mater. Res. **45**, 217 (2015).
[39] V. Hutanu, A. Sazonov, M. Meven, H. Murakawa, Y. Tokura, S. Bordacs, I. Kezsmarki, and B. Nafradi, Phys. Rev. B **86**, 104401 (2012).
[40] L. Ding, C. V. Colin, C. Darie, and P. Bordet, J. Mater. Chem. C **4**, 4236 (2016).
[41] I. Dzyaloshinskii, J. Phys. Chem. Solids **4**, 241 (1958).
[42] T. Moriya, Phys. Rev. **120**, 91 (1960).
[43] T. Zou, Z. Dun, H. Cao, M. Zhu, D. Coulter, H. Zhou, and X. Ke, Appl. Phys. Lett. **105**, 052906 (2014).
[44] T. N. M. Ngo, U. Adem, and T. T. M. Palstra, Appl. Phys. Lett. **106**, 152904 (2015).